



## Adaptive controller for tracking power profile in a fuel cell powered automobile

Panini K. Kolavennu <sup>a</sup>, Srinivas Palanki <sup>b,\*</sup>, David A. Cartes <sup>c</sup>, John C. Telotte <sup>a</sup>

<sup>a</sup> Department of Chemical and Biomedical Engineering, FAMU-FSU College of Engineering, Florida State University, 2525 Pottsdamer Street, Tallahassee, FL 32310-6046, United States

<sup>b</sup> Department of Chemical Engineering, University of South Alabama, 307 University Blvd N, EGLB 244, Mobile, AL 36608-0002, United States

<sup>c</sup> Department of Mechanical Engineering, FAMU-FSU College of Engineering, Florida State University, 2525 Pottsdamer Street, Tallahassee, FL 32310-6046, United States

Received 21 March 2006; received in revised form 17 October 2007; accepted 17 October 2007

---

### Abstract

In this paper, a model reference adaptive controller is designed using the Lyapunov method, for tracking a time varying power profile in an automobile powered by a fuel cell. The adaptability of the controller is tested by implementing the controller on different power profiles which simulate actual power requirement of different road conditions. The performance of the adaptive controller is compared with a conventional PID controller and it is observed that the adaptive controller has superior performance.

© 2007 Elsevier Ltd. All rights reserved.

*Keywords:* Adaptive control; Fuel cell automobile; Power profile

---

### 1. Introduction

Fuel cell power systems for automotive applications have received increased attention in recent years because of their potential for high fuel efficiency and lower emissions [11]. In particular, a fuel cell converts hydrogen and oxygen into water, directly generating electrical energy from chemical energy without being restricted by efficiency limits of the Carnot thermal cycle [5]. This interest in automotive applications has primarily been the result of the breakthroughs made in polymer electrolyte membrane (PEM) fuel cells which have several attractive features such as low operating temperatures (around 80 °C), relatively low cost, simple maintenance requirements, and high efficiency.

For fuel cell systems to operate at power levels comparable to existing internal combustion engines one of the key control issue that should be addressed is the transient

behavior of fuel cell systems. Automobiles are subjected to significant load transitions during operation and the fuel cell system should be able to produce power which can follow this time varying load profile. Hence it is necessary to design a control system which can follow the power demand trajectory which depends on the road profile. A controller tuned for handling city driving may not work for highway driving or for uphill driving. Since it is difficult to consider all the road profiles and driving conditions *a priori*, a controller that can adapt or change its controller settings online depending on the road conditions has the potential to provide better performance.

In this paper, we evaluate the efficiency of a model reference adaptive controller (MRAC) in following a variety of realistic power demand profiles in a fuel cell powered automobile. In Section 2, a brief description of the fuel cell powered automobile is given and a control-oriented dynamic model for this system is presented. In Section 3, the design procedure of MRAC is described and methods to improve robustness by adding deadzone are explained. In Section 4, an adaptive controller is designed and

---

\* Corresponding author. Tel.: +1 850 410 6163; fax: +1 850 410 6150.  
E-mail address: [spalanki@usouthal.edu](mailto:spalanki@usouthal.edu) (S. Palanki).

implemented on the nonlinear model of the fuel cell system. Realistic road conditions are utilized from the ADVISOR [8] software to test the efficacy of the controller. The controller performance is further improved by the use of a Proportional-Derivative (PD) controller. Finally, in Section 5, the major conclusions of this work are presented.

## 2. System description and model development

While there have been significant advances in fuel cell technology, this technology has not seen wide-spread applications in the automotive industry due to the lack of an efficient hydrogen distribution center and the difficulties associated with storing hydrogen onboard an automobile. One option to alleviate these problems is to develop a system that utilizes a commonly available carbon-based hydrogenous fuel such as gasoline or methane to generate the necessary hydrogen *in situ* on an “as needed” basis. Hydrocarbon fuels are relatively easy to store onboard a vehicle and a nationwide infrastructure to supply these fuels already exists.

A schematic of the fuel cell system under consideration is shown in Fig. 1. The two main components of the overall system are (1) the fuel processing subsystem and (2) the power generation subsystem. Methane enters the fuel processing subsystem and is converted to hydrogen. Hydrogen enters the power generation subsystem where it reacts with oxygen in a fuel cell to generate electrical power that drives an electric motor. The fuel processor subsystem consists of three reactors in series: (1) a steam reformer where methane is reformed to a hydrogen rich gas, (2) a water–gas shift reactor where most of the carbon monoxide (CO) is converted to carbon dioxide (CO<sub>2</sub>) and (3) a preferential oxidation reactor where the CO concentration is reduced to less than 100 ppm to avoid poisoning the catalyst in the PEM fuel cell membrane. Using standard reaction engineering principles, the sizes of the reactors and the fuel cell stack

for the system shown in Fig. 1 were determined in a previous paper [4].

Pukrushpan [9] developed and experimentally verified a dynamic model for a PEM fuel cell stack system similar to the one shown in Fig. 1. The model incorporates transient behavior that is important for controller design and analysis. In particular, a time-scale analysis of the various components was conducted and dynamic balances were developed for those operations that relate to automobile operations. Slower dynamics associated with temperature regulation and heat dissipation were ignored. Inertia dynamics along with nonlinear curve fitting of the compressor characteristic map were used to model the compressor. The manifold dynamics were based on lumped-volume filling dynamics. Static models of the air cooler and air humidifier were developed from thermodynamic relations. The fuel cell stack model was composed of four interacting submodels, namely stack voltage, cathode flow, anode flow and membrane hydration. The dynamic equations at the cathode and anode were developed using mass conservation principles and thermodynamic and psychrometric properties of air. All gases were assumed to behave like an ideal gas. Spatial variations in temperature and concentration were ignored. It was assumed that the anode inlet flow rate could be instantaneously adjusted by a valve to maintain the minimum pressure difference between the cathode and the anode. Mass transport of water across the fuel cell membrane was calculated in membrane hydration model. Both water content and mass flow were assumed to be uniform over the surface of the membrane. However, this model developed by Pukrushpan [9] consists of a large number of coupled, nonlinear differential and algebraic equations (DAE) and adaptive control theory cannot be applied directly to this system.

An analysis of this DAE system indicated that this system was of index one and could thus be reduced to a system of ordinary differential equations. After suitable

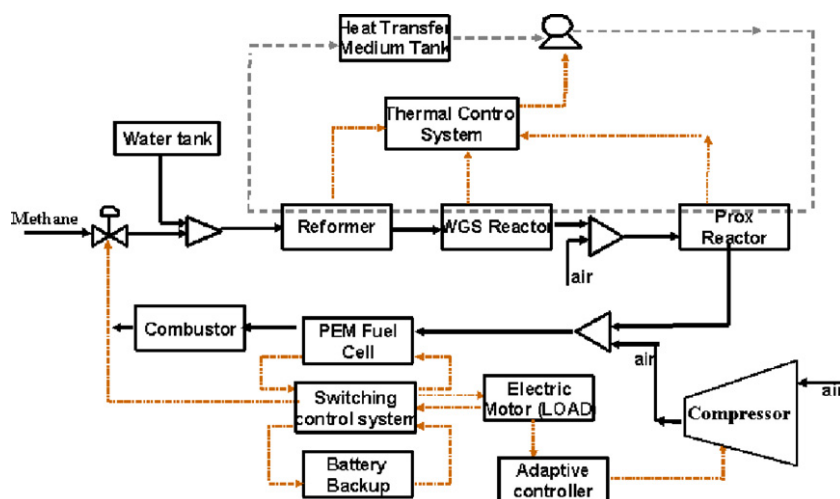


Fig. 1. Schematic of fuel cell system.

substitution of variables, the following reduced model of the fuel cell system was obtained.

*Oxygen balance at the cathode*

$$\begin{aligned} \frac{dm_{O_2}}{dt} = & X_{O_2,in}K_{ca,in} \\ & \times \left( P_{sm} - \frac{(m_{O_2}/M_{O_2} + m_{N_2}/M_{N_2} + m_{v,ca}/M_v)RT_{st}}{V_{ca}} \right) \\ & - \left( \frac{m_{O_2}}{m_{O_2} + m_{N_2} + m_{v,ca}} \right) K_{ca,out} \\ & \times \left( \frac{(m_{O_2}/M_{O_2} + m_{N_2}/M_{N_2} + m_{v,ca}/M_v)RT_{st}}{V_{ca}} - P_{rm} \right) \\ & - \frac{M_{O_2}nI_{st}}{4F} \end{aligned} \quad (1)$$

*Hydrogen balance at the cathode*

$$\begin{aligned} \frac{dm_{H_2}}{dt} = & K_1K_2P_{sm} - K_1 \frac{(m_{H_2}/M_{H_2} + m_{v,an}/M_v)RT_{st}}{V_{an}} \\ & - \frac{M_{H_2}nI_{st}}{2F} \end{aligned} \quad (2)$$

*Nitrogen balance at the cathode*

$$\begin{aligned} \frac{dm_{N_2}}{dt} = & \left( \frac{M_{N_2}}{M_{O_2}} \right) \left( \frac{79}{21} \right) X_{O_2,in}K_{ca,in} \\ & \times \left( P_{sm} - \frac{(m_{O_2}/M_{O_2} + m_{N_2}/M_{N_2} + m_{v,ca}/M_v)RT_{st}}{V_{ca}} \right) \\ & - \left( \frac{m_{N_2}}{m_{O_2} + m_{N_2} + m_{v,ca}} \right) K_{ca,out} \\ & \times \left( \frac{(m_{O_2}/M_{O_2} + m_{N_2}/M_{N_2} + m_{v,ca}/M_v)RT_{st}}{V_{ca}} - P_{rm} \right) \end{aligned} \quad (3)$$

*Compressor balance*

$$\begin{aligned} \frac{dw_{cp}}{dt} = & \frac{\eta_{cm}k_t}{J_{cp}R_{cm}} (v_{cm} - k_v w_{cp}) \\ & - \frac{C_p T_{atm}}{J_{cp} \eta_{cp} W_{cp}} \left( \left( \frac{P_{sm}}{P_{atm}} \right)^{\frac{\gamma-1}{\gamma}} - 1 \right) W_{cp} \end{aligned} \quad (4)$$

*Pressure balance at the supply manifold*

$$\begin{aligned} \frac{dP_{sm}}{dt} = & \left( \frac{\gamma R}{V_{sm}} \right) T_{atm} \left( \frac{P_{sm}}{P_{atm}} \right)^{\frac{\gamma-1}{\gamma}} W_{cp} - \frac{\gamma P_{sm}}{m_{sm}} K_{ca,in} \\ & \times \left( P_{sm} - \frac{(m_{O_2}/M_{O_2} + m_{N_2}/M_{N_2} + m_{v,ca}/M_v)RT_{st}}{V_{ca}} \right) \end{aligned} \quad (5)$$

*Mass balance in the supply manifold*

$$\begin{aligned} \frac{dm_{sm}}{dt} = & W_{cp} - K_{ca,in} \\ & \times \left( P_{sm} - \frac{(m_{O_2}/M_{O_2} + m_{N_2}/M_{N_2} + m_{v,ca}/M_v)RT_{st}}{V_{ca}} \right) \end{aligned} \quad (6)$$

*Pressure balance in the return manifold*

$$\begin{aligned} \frac{dP_{rm}}{dt} = & \frac{RT_{st}}{V_{rm}} \left( K_{ca,out} \right. \\ & \times \left( \frac{(m_{O_2}/M_{O_2} + m_{N_2}/M_{N_2} + m_{v,ca}/M_v)RT_{st}}{V_{ca}} - P_{rm} \right) \\ & - \frac{C_D A_T P_{rm}}{\sqrt{RT_{st}}} \\ & \left. \times \left( \left( \frac{P_{atm}}{P_{rm}} \right)^{\frac{1}{\gamma}} \left( \frac{2\gamma}{\gamma-1} \left( 1 - \left( \frac{P_{atm}}{P_{rm}} \right)^{\frac{\gamma-1}{\gamma}} \right)^{\frac{1}{\gamma}} \right) \right) \right) \end{aligned} \quad (7)$$

*Water balance at the anode*

$$\begin{aligned} \frac{dm_{v,an}}{dt} = & \left( \frac{M_v}{M_{H_2}} \right) \left( \frac{P_v^{sat}}{\frac{(m_{H_2}/M_{H_2} + m_{v,an}/M_v)RT_{st}}{V_{an}} - P_v^{sat}} \right) K_1 \\ & \times \left( K_2 P_{sm} - \frac{(m_{H_2}/M_{H_2} + m_{v,an}/M_v)RT_{st}}{V_{an}} \right) \\ & - \frac{M_v A_{fc} n}{F} n_d I_{st} + \frac{D_w}{t_m} (C_{v,ca} - C_{v,an}) \end{aligned} \quad (8)$$

*Water balance at the cathode*

$$\begin{aligned} \frac{dm_{v,ca}}{dt} = & \left( \frac{\phi_{des} P^{sat}}{P_{sm}} \right) \left( \frac{M_v}{M_a} \right) K_{ca,in} \\ & \times \left( P_{sm} - \frac{(m_{O_2}/M_{O_2} + m_{N_2}/M_{N_2} + m_{v,ca}/M_v)RT_{st}}{V_{ca}} \right) \\ & - \left( \frac{m_{v,an}}{m_{O_2} + m_{N_2} + m_{v,an}} \right) K_{ca,out} \\ & \times \left( \frac{(m_{O_2}/M_{O_2} + m_{N_2}/M_{N_2} + m_{v,ca}/M_v)RT_{st}}{V_{ca}} - P_{rm} \right) \\ & + \left( \frac{M_v n}{2F} \right) I_{st} + \left( \frac{M_v A_{fc} n}{2F} \right) n_d I_{st} - \frac{D_w}{t_m} (C_{v,ca} - C_{v,an}) \end{aligned} \quad (9)$$

where  $m_{O_2}$ ,  $m_{H_2}$  and  $m_{N_2}$  represent the mass of oxygen, hydrogen and nitrogen in the cathode (in kg),  $w_{cp}$  is the compressor speed (in rad/s),  $P_{sm}$  and  $P_{rm}$  are the pressures in the supply manifold and the return manifold respectively (in atm),  $m_{sm}$  is the total mass of gas in the manifold (in kg),  $m_{v,an}$  and  $m_{v,ca}$  represent the mass of water vapor in the anode and cathode respectively (in kg). The variable  $W_{cp}$  represents the air mass flow rate in the compressor (in kg/s) and is determined through a compressor flow map [6]. The remaining parameter values are taken from Pukrushpan [9]. The dynamic model predicts the amount of each gas species in the fuel cell for a given current input,  $I_{st}$ .

The power produced by the fuel cell, which is a function of the current and voltage, is given by the following equation:

$$P = V_{st} I_{st} = (N_c V_c) (i A_c) \quad (10)$$

where  $P$  is the power produced by the fuel cell,  $V_{st}$  is the voltage of the stack which is the product of the number

of cells  $N_c$  and the individual cell voltage  $V_c$ ,  $I_{st}$  is the current drawn from the cell and is the same for each cell and depends on the area of cross section  $A_c$ ,  $i$  is the current density.

The voltage,  $V_{st}$ , resulting from the current,  $I_{st}$ , to the fuel cell model described by Eqs. (1)–(9) is determined by

$$V_{st} = V_0 - V_{act} - V_{ohm} - V_{conc} \quad (11)$$

where  $V_0$  is the open circuit voltage and  $V_{act}$ ,  $V_{ohm}$  and  $V_{conc}$  are activation, ohmic and concentration overvoltages, which represent losses due to various physical and chemical factors. Pukrushpan [9] developed expressions for  $V_0$ ,  $V_{act}$ ,  $V_{ohm}$  and  $V_{conc}$  by fitting experimental data and these are briefly described below. The regressed parameters were obtained from fuel cell polarization data from an automotive propulsion-sized PEM fuel cell stack and thus inefficiencies in the stack are automatically accounted for.

The open circuit voltage is calculated from the Nernst equation as shown below:

$$V_0 = 1.229 - 8.5 \times 10^{-4}(T_{fc} - 298.15) + 4.3085 \times 10^{-5} T_{fc} \left[ \ln \left( \frac{m_{H_2}}{M_{H_2}} \frac{RT_{st}}{V_{ca}} \right) - \frac{1}{2} \ln \left( \frac{m_{H_2}}{M_{H_2}} \frac{RT_{st}}{V_{ca}} \right) \right] \quad (12)$$

The activation overvoltage is calculated from the Tafel equation as shown below:

$$V_{act} = 0.279 - 8.5 \times 10^{-4}(T_{st} - 298.15) + 4.3085 \times 10^{-5} T_{st} \times \left[ \ln \left( \frac{(m_{O_2}/M_{O_2} + m_{N_2}/M_{N_2} + m_{v,ca}/M_v)RT_{st}}{1.01325V_{ca}} \right) - \frac{P_{sat}}{1.01325} \right] + \frac{1}{2} \ln \left( \frac{0.1173((m_{O_2}/M_{O_2} + m_{N_2}/M_{N_2} + m_{v,ca}/M_v)RT_{st})}{1.01325V_{ca}} - \frac{P_{sat}}{1.01325} \right) + (-1.618 \times 10^{-5} T_{st} + 1.618 \times 10^{-2}) \times \left( \frac{m_{O_2}RT_{st}}{0.1173V_{ca}} + P_{sat} \right)^2 + (1.8 \times 10^{-4} T_{fc} - 0.166) \times \left( \frac{m_{O_2}RT_{st}}{0.1173V_{ca}M_{O_2}} + P_{sat} \right) + (-5.8 \times 10^{-4} T_{st} + 0.5736)(1 - e^{10i}) \quad (13)$$

The ohmic overvoltage is calculated from Ohm's law as shown below:

$$V_{ohm} = i \cdot R_{ohm} = i \frac{t_m}{0.7162 \exp \left[ 350 \left( \frac{1}{303} - \frac{1}{T_{st}} \right) \right]} \quad (14)$$

where  $t_m$  is the membrane thickness. The concentration overvoltage is calculated from

$$V_{conc} = i \left( c_2 \frac{i}{2} \right)^2 \quad (15)$$

where  $c_2$  is the following empirical constant:

$$\begin{cases} \text{if } \frac{m_{O_2}RT_{st}}{0.1173V_{ca}} + P_{sat} < 2 \text{ atm,} \\ c_2 = (7.16 \times 10^{-4} T_{fc} - 0.622) \left( \frac{m_{O_2}RT_{st}}{0.1173V_{ca}M_{O_2}} + P_{sat} \right) \\ \quad + (-1.45 \times 10^{-3} T_{fc} + 1.68) \\ \text{else} \\ c_2 = (8.66 \times 10^{-5} T_{fc} - 0.068) \left( \frac{m_{O_2}RT_{st}}{0.1173V_{ca}M_{O_2}} + P_{sat} \right) \\ \quad + (-1.6 \times 10^{-4} T_{fc} + 0.54) \end{cases} \quad (16)$$

Thus, the dynamic nonlinear equations represented by Eqs. (1)–(9) can be used in combination with Eq. (11) to determine the relationship between current  $I_{st}$  and the voltage  $V_{st}$  as a function of time. Then, Eq. (10) can be used to determine the power generated by the fuel cell at any given time.

### 3. Review of model reference adaptive controller

Adaptive control systems were first developed in the early 1950s for the design of autopilots for high performance aircrafts. The two types of adaptive controllers which are generally used are the Model Reference Adaptive Controller (MRAC) suggested by Whitaker et al. [10] and the Adaptive Pole Placement Controller (APPC) suggested by Kalman [3]. MRAC schemes using a Lyapunov approach were designed and analyzed by Narendra et al. [7]. Initially developed for autopilot systems, adaptive controllers now find applications in wide areas like robotic arm manipulators, engine control, chemical reactors and distillation columns. The advances in adaptive control theory coupled with the availability of microprocessors has been the main driving force behind the development of practical adaptive control systems.

The objective of MRAC is to find the feedback control law that changes the structure and dynamics of the plant so that its input/output (I/O) properties are exactly the same as those of a reference model. The structure of a MRAC scheme for a linear time invariant, Single Input Single Output (SISO) plant is shown in Fig. 2. Here  $W_m(s)$  is the transfer function of the reference model,  $r(t)$  a given reference input signal,  $y_m(t)$  the output of the reference model and  $y(t)$  is the plant output. The feedback controller denoted by  $C(\theta_c^*)$  is designed so that all signals are bounded and the closed loop plant transfer function from  $r$  to  $y$  is equal to  $W_m(s)$ .  $\theta_c$  is the set of parameters that are adap-

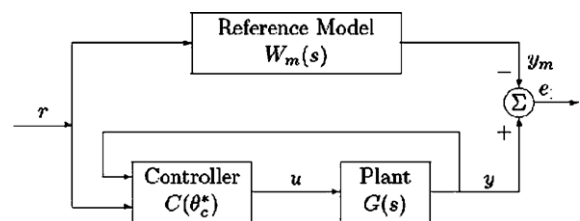


Fig. 2. Model reference adaptive control.

tively estimated. This transfer function matching guarantees that for any given reference input  $r(t)$ , the tracking error  $e = y - y_m$ , which represents the deviation of the plant output from the desired trajectory  $y_m$ , converges to zero with time.

### 3.1. Design procedure

In this subsection, the design procedure of MRAC will be reviewed. In particular, design equations for feedback control of a second order system will be developed to track a first order reference model. In a succeeding section, the nonlinear model represented by Eqs. (1)–(9) will be approximated by a second order linear model for developing the appropriate adaptive controller, which will then be implemented on the nonlinear model represented by Eqs. (1)–(9).

Consider a SISO second order linear dynamic system that can be represented as

$$\begin{aligned} \dot{x} &= Ax + bu \\ y &= cx \end{aligned} \quad (17)$$

where  $x$  represents the system state,  $A$  is a  $2 \times 2$  constant matrix,  $b$  and  $c$  are constant vectors of dimension 2, and  $u$  represents the control effort. The reference model is chosen as

$$\begin{aligned} \dot{x}_m &= -a_m x_m + b_m r \\ y_m &= x_m \end{aligned} \quad (18)$$

where  $r$  is the setpoint and  $a_m, b_m$  are positive constants known *a priori*.

The control effort  $u$  is given by

$$u = -kx + lr \quad (19)$$

Substituting the above equation into Eq. (17) yields

$$\begin{aligned} \dot{x} &= (A - bk)x + blr \\ y &= cx \end{aligned} \quad (20)$$

The objective is to find a feedback control law so that the plant I/O properties are exactly the same as those of the reference model. In order to achieve this the error is defined as the difference between the plant output and the reference model output.

$$e = y - y_m \quad (21)$$

By taking the time derivative of  $e$

$$\dot{e} = \dot{y} - \dot{y}_m = c(A - bk)x + blr + a_m x_m - b_m r \quad (22)$$

Eliminating  $x_m$  from Eq. (22) by substituting  $x_m = cx - e$  we have

$$\dot{e} = -a_m e + (c(A - bk) + a_m c)x + (bl - b_m)r \quad (23)$$

For the adaptive controller an adaptation mechanism for  $k$  and  $l$  has to be developed such that the error is minimized. Let the optimal values of  $k$  and  $l$  be represented by  $k^*$  and  $l^*$ . If we set

$$\begin{aligned} k^* &= \frac{cA + a_m c}{cb} \\ l^* &= \frac{b_m}{cb} \end{aligned} \quad (24)$$

then,  $\dot{e}$  will decay exponentially in Eq. (23). Since  $A, b$ , and  $c$  are not precisely known, the optimal values  $k^*$  and  $l^*$  cannot be calculated exactly. Thus, we start with an initial guess  $k$  and  $l$  for the adaptive controller.

$$\begin{aligned} \tilde{k} &= k - k^* \\ \tilde{l} &= l - l^* \end{aligned} \quad (25)$$

Now Eq. (23) can be rewritten as

$$\dot{e} = -a_m e - cb\tilde{k}x + cb\tilde{l}r \quad (26)$$

The following positive definite candidate Lyapunov function is chosen:

$$V(e, \tilde{k}, \tilde{l}) = \frac{1}{2}e^2 + \frac{cb}{2\gamma_1}\tilde{k}\tilde{k}^T + \frac{b}{2\gamma_2}\tilde{l}^2 \quad (27)$$

where  $\gamma_1$  and  $\gamma_2$  are tuning parameters whose sign is the same as that of the scalar  $cb$ . The derivative of Eq. (27) gives

$$\dot{V} = -a_m e^2 + \left(\frac{cb}{\gamma_1}\dot{\tilde{k}}\tilde{k}^T - cbe\tilde{k}x\right) + \left(cbe\tilde{l}r + \frac{cb}{\gamma_2}\dot{\tilde{l}}\right) \quad (28)$$

To ensure stability, Eq. (28) must be negative definite [2]. The only way to ensure this is to set the second and third term of Eq. (28) to zero. This produces the adaptive law

$$\begin{aligned} \dot{\tilde{k}}^T &= \gamma_1 ex \\ \dot{\tilde{l}} &= -\gamma_2 er \end{aligned} \quad (29)$$

where  $\gamma_1$  and  $\gamma_2$  are tuning parameters. The initial conditions  $l(0)$  and  $k(0)$  are chosen by trial and error.

### 3.2. Adaptive controller with deadzone

In cases where there are noisy outputs, it is necessary to add robustness to the controller. In the presence of unmodeled disturbances there are several instability mechanisms which have to be addressed, such as parameter drift, high gain instability and instability resulting from fast adaption. Ioannou and Kokotovic [1] addressed the issue of instability in the presence of unmodeled dynamics and bounded disturbances. Different methods, such as leakage modification, parameter projection and deadzone are used as modifications to the Lyapunov approach to ensure stability. To avoid phenomena such as bursting (i.e., large errors relative to the level of the disturbance at steady state and over short intervals of time) that may arise in the case of the leakage modification and projection, a deadzone is used. Another important property of the adaptive law with deadzone is that it guarantees parameter convergence [2].

The Lyapunov design outlined above is modified such that the values of  $\tilde{k}, \tilde{l}$  remain same as Eq. (29) as long as

the disturbance is bounded. If the error  $e$  is less than the bounded disturbance  $\tilde{k}$  and  $\tilde{l}$  can be equated to zero.

$$\dot{\tilde{k}} = 0 \quad |e| \leq \frac{d_0}{a_m} \quad (30)$$

$$\dot{\tilde{l}} = 0 \quad |e| \leq \frac{d_0}{a_m} \quad (31)$$

In the above equations,  $d_0/a_m$  represents a bounded disturbance. The principal idea behind the dead zone is to monitor the size of the estimation error and adapt only when the estimation error is large relative to the modeling error. In essence, for some bounded disturbance  $d_0$ , the adaptation law can be turned on or off depending on the value of the error. Moreover, the practical benefit for implementing a deadzone is that this procedure saves actuator energy because the controller is not always in use.

#### 4. MRAC design for fuel cell stack

In this section, the MRAC design procedure is designed for the fuel cell system. First, the nonlinear model developed in Section 2 is linearized to a second order model. Then, the MRAC procedure is utilized to design an adaptive controller that computes the necessary input moves to track a given power profile. Realistic power profiles that vary with road conditions are generated from the ADVISOR software developed by NREL [8]. This adaptive controller is implemented on the nonlinear model developed in Section 2 and the efficacy of the controller to track a variety of different road profiles. This performance is compared with a standard PID controller. Finally, it is shown that the adaptive controller performance improves if derivative action is added.

##### 4.1. Linearization

The nonlinear model represented by Eqs. (1)–(9) was linearized around a current demand of 100 A and a stack voltage of 247 V. The following transfer function,  $G_p$ , between current demand and voltage produced by the fuel cell stack adequately represented a step change of 20 A.

$$G_p = \frac{-390.78}{s^2 + 27.291s + 2068.8} \quad (32)$$

When there is an increase in current demand the operating current density of the fuel cell increases. From the fuel cell polarization curve [4] it is evident that with increase in current density there is a decrease in voltage. Hence any increase in current demand results in a decrease in the voltage of the stack. The power output from the fuel cell is defined as the product of the current and the voltage produced by the stack. This linearized model is used for designing an adaptive controller. While this linearization is clearly valid only in a small range of current changes, it is shown in the succeeding section that the adaptive controller, when implemented on the *nonlinear* system

represented by Eqs. (1)–(9) and (11), is able to successfully track several realistic power profiles.

##### 4.2. Realistic power profile

To get a realistic power vs time profile, the power profile for a small car was obtained from an existing speed vs time profile using the ADVISOR software package [8]. The urban dynamometer driving schedule (UDDS), which is designed for light duty vehicle testing in city driving conditions has been used. The speed versus time and the corresponding force versus time profiles are shown in Fig. 3.

The force profile has both positive and negative values denoting the acceleration and deceleration phases of the car. The power requested by the engine is a product of the speed and force. During acceleration the force is positive and since the speed is always positive the power demand is positive and this power demand should be met by the power generation system. During deceleration the force and hence the power requested is negative and since this is handled by the braking system the power requested from the power generation subsystem is zero. Hence the negative power demand is equated to zero and the corresponding power profile is shown in Fig. 4. As seen from this figure the power profile changes continuously with time and a controller should be designed such that it follows the trajectory of the power profile as closely as possible.

##### 4.3. MRAC simulation results

The linearized model used for the controller design is given by Eq. (32). The input to the model is the current demand and the output from the model is the voltage. The power output is obtained as a product of the current and the voltage. To develop the adaptive controller, a reference model with  $a_m = 1$  and  $b_m = 0.023$  was chosen. The adaptive controller was implemented in MATLAB/Simu-

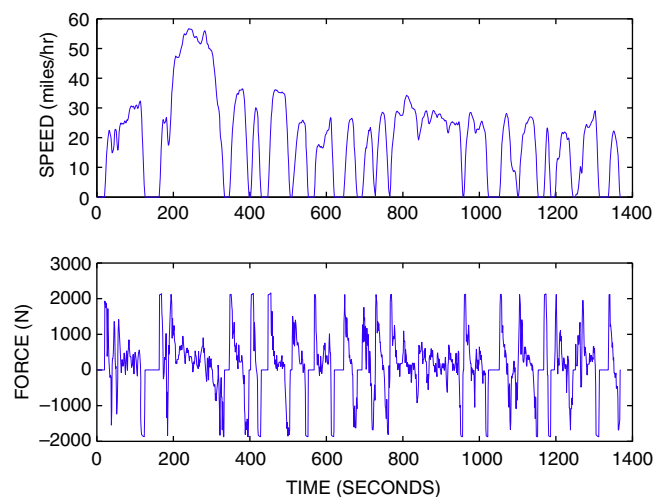


Fig. 3. Speed vs time profile and Force vs time profile for UDDS.

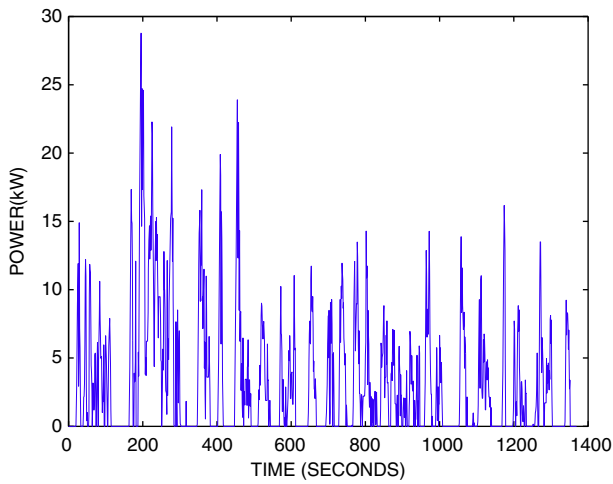


Fig. 4. Power vs time profile for UDDS.

link as shown in Fig. 5. The tuning parameters  $\gamma_1$ ,  $\gamma_2$  and the initial guesses for  $l(0)$  and  $k(0)$  were calculated on a trial and error basis by varying the parameter values over a range and obtaining the values which give the best performance. The tuning parameters  $\gamma_1$  and  $\gamma_2$  were set to  $10^{-9}$ . The performance of the adaptive controller was compared with that of a conventional PID controller. For the PID controller, parameters  $K_c$ ,  $\tau_i$ ,  $\tau_d$  were varied for a range of  $10^{-1}$ – $10^{-4}$  and the values for which the lowest integrated time averaged error was obtained were  $K_c = 0.051$ ,  $\tau_i = 0.001$ ,  $\tau_d = 0.0001$ . For implementing the deadzone, the bounded disturbance is chosen to be 0.01 kW. To make a quantitative comparison between the adaptive controller and a PID controller, the integrated time averaged error (ITAE) was calculated by the following equation:

$$ITAE = \sum_{i=0}^n \frac{t_i |e_i(t)|}{n} \quad (33)$$

where  $n$  stands for the number of time steps and  $e_i$  is the error at time  $t_i$ .

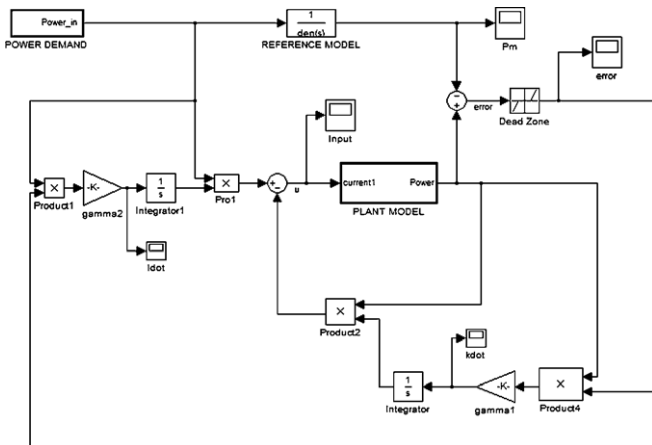


Fig. 5. Simulink diagram of the adaptive controller.

The PID controller and the adaptive controller were implemented on the nonlinear model. The errors obtained for the UDDS profile are shown in Fig. 6. The adaptive controller error has a larger undershoot compared to the PID controller but the error comes back to zero quicker than the PID controller. The ITAE obtained when implemented on the nonlinear models for the two controllers is given in Table 1. It is observed that the MRAC performs better than the PID for the UDDS profile. Note that the parameters of both controllers were fine tuned assuming the power profile was known *a priori*. However, an important aspect of designing a controller for an automotive purpose is we do not know the trajectory of the power profile *a priori* and so the controller tuned for one profile should work for several other typical road profiles. The controller designed for the UDDS profile was implemented on a US06-HWY (2002) profile which simulates highway driving instead of city driving represented by UDDS. This cycle has been created to provide a very short high speed highway test cycle and the speed and power profiles are shown in Fig. 7.

When the US06-HWY profile is used on the controllers designed for the UDDS profile, the PID controller failed as the system became unstable. On the other hand, the adaptive controller works well as shown in Table 1.

#### 4.4. MRAC with derivative action

The performance of the adaptive controller is better than that of the PID controller; however, the adaptive

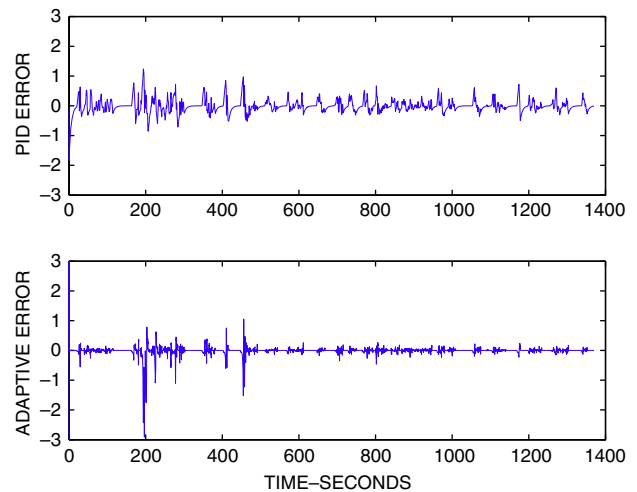


Fig. 6. Error obtained (kW) for the PID controller and adaptive controller.

Table 1  
Average ITAE error in kW s

Profile	PID	MRAC
UDDS	91.46	40.5
US06-HWY	Unstable	55.6

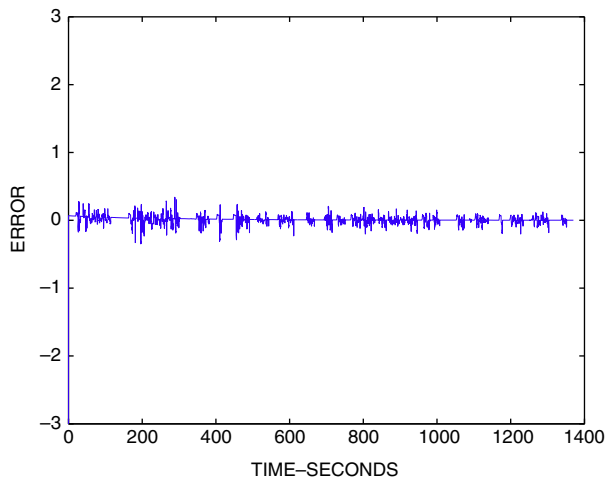


Fig. 7. Speed and power profiles for the US06-HWY driving cycle.

controller takes some time to adjust to the changes in the profiles. This is because the adaptive controller tries to approximate the actual nonlinear model to a linear first order model and the calculates appropriate control actions to make the closed loop system follow the specified linear first order reference model. The actual nonlinear model response more closely represents a second order process. The performance of the adaptive controller can be improved by adding some derivative action, i.e., using a PD controller in conjunction with the adaptive controller. Note that for the PD controller, the error is defined as difference between the setpoint and the plant output. For the adaptive controller the error is defined as deviation of the plant output from the reference model output.

The following analysis for the stability and adaptation law for the combined PD and adaptive controllers is along the lines of Ioannou and Sun [2]. Consider the plant equation given by a second order transfer function

$$y_p = G_p(s)u_p, \quad \text{where} \quad (34)$$

$$G_p(s) = \frac{b}{s^2 + a_1s + a_2} \quad (35)$$

If a PD controller is added to adaptive action as shown in Fig. 8, the new control input to the system is given by

$$u_p = \bar{k}y_p + \bar{l}r + k_c(y_p - r) + K_d s(y_p - r) \quad (36)$$

Without loss in generality, this can be written as

$$u_p = k^*y_p + l^*r + k_d s y_p - k_d s r \quad (37)$$

Substituting this value of  $u_p$  into Eq. (34), we can calculate the closed loop transfer function between  $y_p$  and  $r$  as

$$(s^2 + a_1s + a_2)y_p = b(k^*y_p + l^*r + k_d s y_p - k_d s r) \quad (38)$$

This implies

$$y_p = \frac{b(l^* - s k_d)}{s^2 + (a_1 - k_d b)s + (a_2 - b k^*)} r \quad (39)$$

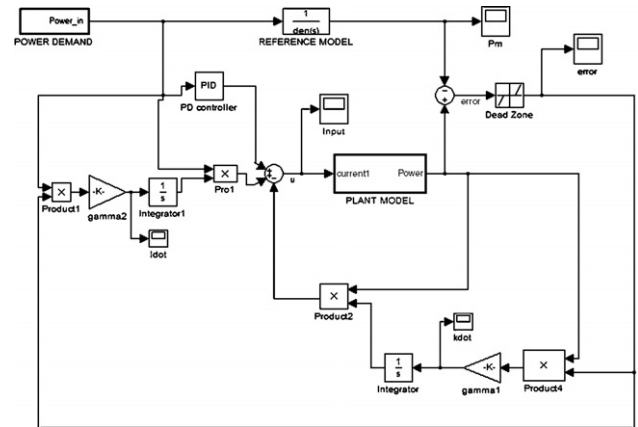


Fig. 8. Adaptive controller with derivative action.

The control objective is to track the reference model output

$$y_m = \frac{b_m}{s + a_m} r \quad (40)$$

Equating the right hand sides of Eqs. (40) and (39) we get

$$\frac{b(l^* - s k_d)}{s^2 + (a_1 - k_d b)s + (a_2 - b k^*)} r = \frac{b_m}{s + a_m} r; \quad \text{which implies} \quad (41)$$

$$(-k_d b)s^2 + b(l^* - a_m k_d)s + a_m l^* b = b_m s^2 + b_m(a_1 - k_d b)s + a_2 - b k^* \quad (42)$$

Equating the coefficients of  $s^n$  on both sides we have the optimal values for  $k_d, l^*, k^*$

$$k_d = \frac{-b_m}{b} \quad (43)$$

$$l^* = \frac{b_m}{b}(a_1 + b_m - a_m) \quad (44)$$

$$k^* = \frac{a_2 - a_m l^* b}{b} \quad (45)$$

The optimal values of  $k_d, l^*, k^*$  when substituted in Eq. (38) ensure that the plant output follows the model output. Hence if  $k^*$  and  $l^*$  are exactly known then  $y_p = y_m$  and we have

$$(s^2 + a_1s + a_2)y_m = b(k^*y_p + l^*r + k_d s y_p - k_d s r) \quad (46)$$

In reality,  $k^*$  and  $l^*$  are not known. If  $k$  and  $l$  are estimates of  $k^*$  and  $l^*$ , then

$$(s^2 + a_1s + a_2)y_p = b(ky_p + lr + k_d s y_p - k_d s r) \quad (47)$$

Subtracting Eq. (46) from Eq. (47) and replacing  $y_p - y_m$  with  $e$ , we have

$$(s^2 + a_1s + a_2)e = b(\tilde{k}y_p + \tilde{l}r), \quad \text{where} \quad (48)$$

$$\tilde{k} = k - k^*; \quad \tilde{l} = l - l^*$$

This can be expressed in state space form as

$$\dot{X} = A_c X + B_c \tilde{\theta}^T \omega \quad (49)$$

$$e = C_c^T X \quad (50)$$

where

$$A_c = \begin{pmatrix} 0 & 1 \\ -a_2 & -a_1 \end{pmatrix}; \quad Bc = \begin{pmatrix} 0 \\ b \end{pmatrix}; \quad C_c = \begin{pmatrix} 1 \\ 0 \end{pmatrix};$$

$$X = \begin{pmatrix} e \\ \dot{e} \end{pmatrix}; \quad \tilde{\theta} = \begin{pmatrix} \tilde{k} \\ \tilde{l} \end{pmatrix}; \quad \omega = \begin{pmatrix} y_p \\ r \end{pmatrix}$$

Eq. (49) can be written as

$$\dot{X} = A_c X + \overline{B}_c \rho^* \tilde{\theta}^T \omega; \quad \text{where } \overline{B}_c = B_c l^*; \quad \rho^* = 1/l^* \quad (51)$$

$$e = C_c^T X \quad (52)$$

Consider the Lyapunov-like function

$$V(\tilde{\theta}, X) = \frac{X^T P_c X}{2} + \frac{\tilde{\theta}^T \Gamma^{-1} \tilde{\theta}}{2} |\rho^*| \quad (53)$$

where  $\Gamma = \Gamma^T > 0$  and  $P_c = P_c^T > 0$  and satisfies the algebraic equations

$$P_c A_c + A_c^T P_c = -q q^T - v_c L_c \quad (54)$$

$$P_c \overline{B}_c = C_c \quad (55)$$

where  $q$  is a vector,  $L_c = L_c^T > 0$  and  $v_c > 0$  is a small constant, that are implied by the Meyer–Kalman–Yakubovich (MKY) lemma [2]. The time derivative  $\dot{V}$  of  $V$  along the solution of Eq. (51) is given by

$$\begin{aligned} \dot{V} = & -\frac{X^T q q^T X}{2} - \frac{v_c}{2} X^T L_c X + X^T P_c \overline{B}_c \rho^* \tilde{\theta}^T \omega \\ & + \tilde{\theta}^T \Gamma^{-1} \dot{\tilde{\theta}} |\rho^*| \end{aligned} \quad (56)$$

Since  $X^T P_c \overline{B}_c = X^T C_c = [C_c^T X]^T = e$  and  $\rho^* = |\rho^*| \text{sgn}(\rho^*)$ , we can make  $\dot{V} \leq 0$  by choosing

$$\dot{\tilde{\theta}} = \dot{\tilde{\theta}} = \Gamma e \omega \text{sgn}(\rho^*) \quad (57)$$

which leads to

$$\dot{V} = -\frac{X^T q q^T X}{2} - \frac{v_c}{2} X^T L_c X \quad (58)$$

which is negative definite. Note that Eq. (57) is same as the adaptation law Eq. (24) used in the previous section. Hence, using the same adaptation mechanism as outlined in the previous section, we can ensure stability as well as improve the performance by adding the PD controller.

The derivative controller is designed and implemented on the nonlinear model for the two profiles discussed before, i.e., the UDDS and the US HWY06 profiles. Fig. 9 shows the error for the UDDS profile when the adaptive controller with derivative action is implemented. The adaptive controller with derivative action performs better than the adaptive controller as shown in Table 2.

The UDDS and US06-HWY profiles considered in the above sections were taken from a database of test procedures, developed by the Environmental Protection Agency. The Environmental Protection Agency (EPA) reviews and revises as necessary the regulations governing the Federal Test Procedures (FTP) to insure that vehicles are tested under circumstances which reflect the actual current

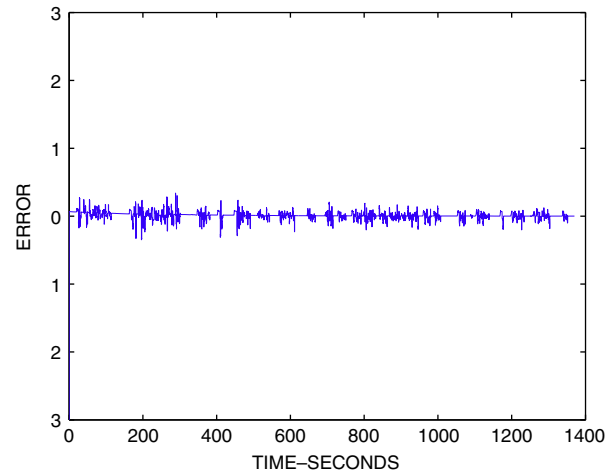


Fig. 9. Error vs time plot for the adaptive controller with derivative action (UDDS profile).

Table 2  
ITAE error for the adaptive controller with the derivative action

Controller	UDDS profile (ITAE)	US06-HWY profile (ITAE)
Adaptive	40.5	55.6
Adaptive with derivative	15.6	31.94

Table 3  
Performance of MRAC on different road profiles

Profile or cycle	ITAE error
UDDS	15.6
US06	31.94
Highway fuel economy test	11.09
Extra urban driving cycle	8.20
Indian highway profile	10.20

driving conditions under which motor vehicles are used, including conditions relating to fuel, temperature, acceleration, and altitude. The adaptive controller was tested on a variety of profiles. The controller was designed for the UDDS profile and the same settings were employed for the remaining profiles. The results are shown in Table 3. It is observed that the adaptive controller with derivative action is able to track power profiles resulting from a wide variety of road conditions.

## 5. Conclusions

A model reference adaptive controller was designed based on the Lyapunov approach and was shown to perform better than a conventional PID controller for a variety of different power profiles. Robustness of the controller was improved by adding a discontinuous deadzone. The adaptability of the controller was tested by implementing the controller on different power profiles which simulate actual power requirement of different road conditions. A PD

controller was added to the adaptive controller and it was shown that using the same adaptation mechanism the performance of the controller is enhanced.

## References

- [1] P.A. Ioannou, P.V. Kokotovic, Instability analysis and improvement of robustness of adaptive control, *Automatica* 20 (5) (1984) 583–594.
- [2] P. Ioannou, J. Sun, *Robust Adaptive Control*, Prentice Hall Inc., 1996.
- [3] R.E. Kalman, Design of a self optimizing control system, *Transaction of the ASME* 468 (1958) 80.
- [4] P.K. Kolavennu, J.C. Telotte, S. Palanki, Design of a fuel cell power system for automotive applications, *International Journal of Chemical Reactor Engineering* 4 (2006) A19, <Available at: <http://www.bepress.com/ijcre/vol4/A19>>.
- [5] J. Larminie, A. Dicks, *Fuel Cell Systems*, Wiley, New York, 2000.
- [6] P. Moraal, I. Kolmanovsky, Turbocharger modeling for automotive control applications, in: *Proc. SAE Conf.*, 1999-01-0908, 1999.
- [7] K.S. Narendra, Y.H. Lin, L.S. Valavani, Stable adaptive controller design, part II: proof of stability, *IEEE Transactions on Automatic Control* 25 (3) (1980) 440–448.
- [8] National Renewable Energy Laboratory, *ADVISOR (Advanced Vehicle Simulator)*, 2002.
- [9] J.T. Pukrushpan, *Modeling and Control of Fuel Cell Systems and Fuel Processors*, PhD thesis, The University of Michigan, Ann Arbor, 2003.
- [10] H.P. Whitaker, J. Yamron, A. Kezer, *Design of Model Reference Adaptive Control Systems for Aircraft, R-164*, Instrumentation Laboratory, MIT, Cambridge, Massachusetts, 1958.
- [11] J.M. Zalc, D.G. Loffler, Fuel processing for PEM fuel cells: transport and kinetic issues of system design, *J. Power Sources* 111 (2002) 58–64.